

REPORT DOCUMENTATION PAGE			Form Approved OMB NO. 0704-0188		
<p>The public reporting burden for this collection of information is estimated to average 1 hour per response, including the time for reviewing instructions, searching existing data sources, gathering and maintaining the data needed, and completing and reviewing the collection of information. Send comments regarding this burden estimate or any other aspect of this collection of information, including suggestions for reducing this burden, to Washington Headquarters Services, Directorate for Information Operations and Reports, 1215 Jefferson Davis Highway, Suite 1204, Arlington VA, 22202-4302. Respondents should be aware that notwithstanding any other provision of law, no person shall be subject to any penalty for failing to comply with a collection of information if it does not display a currently valid OMB control number. PLEASE DO NOT RETURN YOUR FORM TO THE ABOVE ADDRESS.</p>					
1. REPORT DATE (DD-MM-YYYY) 23-07-2015		2. REPORT TYPE Conference Proceeding		3. DATES COVERED (From - To) -	
4. TITLE AND SUBTITLE Towards direct simulations of counterflow flames with consistent numerical differential-algebraic boundary conditions			5a. CONTRACT NUMBER W911NF-11-1-0398		
			5b. GRANT NUMBER		
			5c. PROGRAM ELEMENT NUMBER 611102		
6. AUTHORS Panayotis D. Kourdis, Josette Bellan			5d. PROJECT NUMBER		
			5e. TASK NUMBER		
			5f. WORK UNIT NUMBER		
7. PERFORMING ORGANIZATION NAMES AND ADDRESSES California Institute of Technology 1200 E. California Blvd. Pasadena, CA 91125 -0001			8. PERFORMING ORGANIZATION REPORT NUMBER		
9. SPONSORING/MONITORING AGENCY NAME(S) AND ADDRESS (ES) U.S. Army Research Office P.O. Box 12211 Research Triangle Park, NC 27709-2211			10. SPONSOR/MONITOR'S ACRONYM(S) ARO		
			11. SPONSOR/MONITOR'S REPORT NUMBER(S) 58744-EG.14		
12. DISTRIBUTION AVAILABILITY STATEMENT Approved for public release; distribution is unlimited.					
13. SUPPLEMENTARY NOTES The views, opinions and/or findings contained in this report are those of the author(s) and should not be construed as an official Department of the Army position, policy or decision, unless so designated by other documentation.					
14. ABSTRACT A new approach for the formulation of boundary conditions for the counterflow configuration is presented. Upon discretization of the steady-state Navier-Stokes equations at the inflow boundaries, numerically algebraic equations are imposed as boundary conditions, while upon discretization of the unsteady Navier-Stokes equations at the outflow, differential boundaries result. It is demonstrated for symmetric potential flow that the resulting numerical differential-algebraic boundary conditions are suitable to account for the multi-directional character of the flow at the boundaries of the counterflow configuration.					
15. SUBJECT TERMS counterflow laminar flame model					
16. SECURITY CLASSIFICATION OF:		17. LIMITATION OF ABSTRACT	15. NUMBER OF PAGES	19a. NAME OF RESPONSIBLE PERSON	
a. REPORT	b. ABSTRACT			c. THIS PAGE	Josette Bellan
UU	UU	UU		19b. TELEPHONE NUMBER 818-354-6959	

Report Title

Towards direct simulations of counterflow flames with consistent numerical differential-algebraic boundary conditions

ABSTRACT

A new approach for the formulation of boundary conditions for the counterflow configuration is presented. Upon discretization of the steady-state Navier-Stokes equations at the inflow boundaries, numerically algebraic equations are imposed as boundary conditions, while upon discretization of the unsteady Navier-Stokes equations at the outflow, differential boundaries result. It is demonstrated for symmetric potential flow that the resulting numerical differential-algebraic boundary conditions are suitable to account for the multi-directional character of the flow at the boundaries of the counterflow configuration.

Conference Name: 9th US National Combustion Meeting

Conference Date: May 18, 2015

9th US National Combustion Meeting
Organized by the Central States Section of the Combustion Institute
May 17-20, 2015
Cincinnati, Ohio

Towards direct simulations of counterflow flames with consistent numerical differential-algebraic boundary conditions

*P. D. Kourdis*¹ and *J. Bellan*^{1,2}

¹*California Institute of Technology, Pasadena, California 91125, USA*

²*Jet Propulsion Laboratory, California Institute of Technology, Pasadena, California, 91109-8099, USA*

A new approach for the formulation of boundary conditions for the counterflow configuration is presented. Upon discretization of the steady-state Navier-Stokes equations at the inflow boundaries, numerically algebraic equations are imposed as boundary conditions, while upon discretization of the unsteady Navier-Stokes equations at the outflow, differential boundaries result. It is demonstrated for symmetric potential flow that the resulting numerical differential-algebraic boundary conditions are suitable to account for the multi-directional character of the flow at the boundaries of the counterflow configuration.

Keywords: *two-dimensional counterflow flames; high-pressure counterflow flames*

1 Introduction

The counterflow configuration provides a comprehensive framework for studying the characteristics of non-premixed laminar and turbulent flame problems [1, 2, 3, 4, 5, 6]. However, apart from the simplified one-dimensional spatial models, the fidelity of direct numerical simulations (DNSs) for the counterflow configuration in terms of robustness/accuracy exhibit significant sensitivity to the boundary condition (BC) treatment [7, 8, 9]. This behavior is mainly due to the multi-directional character of the flow at the boundaries which must be properly accounted by the BCs. To mitigate this problem, Yoo et al. [7] developed improved BCs based on the Navier-Stokes Characteristic Boundary Conditions [10] (NSCBCs) for laminar and turbulent counterflow flames. The major improvement consisted in introducing the (no-longer negligible) transverse terms into the Locally One Dimensional Inviscid (LODI) relations in order to capture the multi-dimensional effects at the inflow/outflow boundaries. However, two major shortcomings can also be identified with the improved NSCBCs. First, they preserve the use of relaxation coefficients entering the improved LODI relations and these coefficients are problem specific. These coefficients provide an optimal balance between maintaining the prescribed upstream values for the inflow variables and reducing spurious wave reflections, and usually must be determined through a trial and error process; this is an expensive, time-consuming procedure. Second, once derived for real-gas, the implementation of these revised NSCBCs adds a considerable computational cost.

In this work, we adopt a totally different approach for constructing BCs for the counterflow configuration that results in a very concise framework. In particular, we combine the steady-state Navier-Stokes equations with an initial flow of potential type to construct numerically consistent

algebraic BCs at the inflow boundaries. The structure of the paper is as follows. First, the governing equations of the problem are presented. A detailed discussion on the construction of the initial profile of the flow follows. Then, the new inflow and outflow boundary conditions are provided. The specifics regarding the numerical implementation follows. Next, the validation of the proposed numerical differential-algebraic BCs is performed. Finally, a summary is given.

2 Governing Equations

2.1 The Navier-Stokes equations

The Navier-Stokes (NS) equations for a compressible reacting multicomponent mixture of N species expressed in terms of the conservative variables $\tilde{\mathbf{U}} = [\tilde{U}_m]$ ($m = 1, \dots, N + 4$) can be cast in compact form as

$$\frac{\partial \tilde{\mathbf{U}}}{\partial t} + \frac{\partial \mathbf{F}^i}{\partial x_i} = \tilde{\mathbf{C}}, \quad (1)$$

where $\mathbf{F}^i = [F_m^i]$ ($m = 1, \dots, N + 4$) denotes the flux vector of the conservative variables along the i -th direction, i.e.

$$\mathbf{F}^i \equiv [\rho u_i, \rho u_1 u_i + p \delta_{1i}, \rho u_2 u_i + p \delta_{2i}, \rho u_3 u_i + p \delta_{3i}, \rho u_i Y_1, \dots, \rho u_i Y_{N-1}, (\rho e_t + p) u_i]^T, \quad (2)$$

and the vector $\tilde{\mathbf{C}} = [C_m]$ ($m = 1, \dots, N + 4$) is defined as

$$\tilde{\mathbf{C}} \equiv [0, \frac{\partial \tau_{1j}}{\partial x_j}, \frac{\partial \tau_{2j}}{\partial x_j}, \frac{\partial \tau_{3j}}{\partial x_j}, -\frac{\partial J_{1j}}{\partial x_j} + \dot{\omega}_1, \dots, -\frac{\partial J_{N-1j}}{\partial x_j} + \dot{\omega}_{N-1}, -\frac{\partial q_j}{\partial x_j} + \frac{\partial (\tau_{ij} u_i)}{\partial x_j}]^T. \quad (3)$$

The usual notation applies in that the indices i and j follow the summation convention, t is time, x_j is the j -th spatial coordinate, ρ is the mass density of the fluid, u_j is the j -th component of the velocity vector, Y_n is the mass fraction of species n , p is the pressure, $e_t = e + \frac{1}{2} u_i u_i$ is the total specific energy (e denotes the specific internal energy), J_{nj} is the j -th component of the mass flux vector \mathbf{J}_n of species n , q_j is the j -th component of the heat flux vector \mathbf{q} and $\dot{\omega}_n$ is the mass reaction rate of species n . Finally, τ_{ij} is the Newtonian viscous stress tensor

$$\tau_{ij} = \mu \left(\frac{\partial u_i}{\partial x_j} + \frac{\partial u_j}{\partial x_i} - \frac{2}{3} \frac{\partial u_k}{\partial x_k} \delta_{ij} \right), \quad (4)$$

where μ is the dynamic viscosity of the mixture and δ_{ij} is the Kronecker delta. Body forces have been neglected in the present equations.

The species-mass and heat fluxes have been given in detail elsewhere [11] and their expressions are based on the fluctuation-dissipation theory [12, 13, 14]. The mixing rules employed for the computation of the mass diffusion coefficients and thermal diffusion factors have been derived by Harstad and Bellan [15] and are based on the conjunction of nonequilibrium thermodynamics [12] in the limit of low pressure and Grad's 13-moment theory [16].

2.2 Transport properties

Transport properties were computed according to the most up-to-date methods [15, 17, 18, 19], an example being provided in Masi et al. [11].

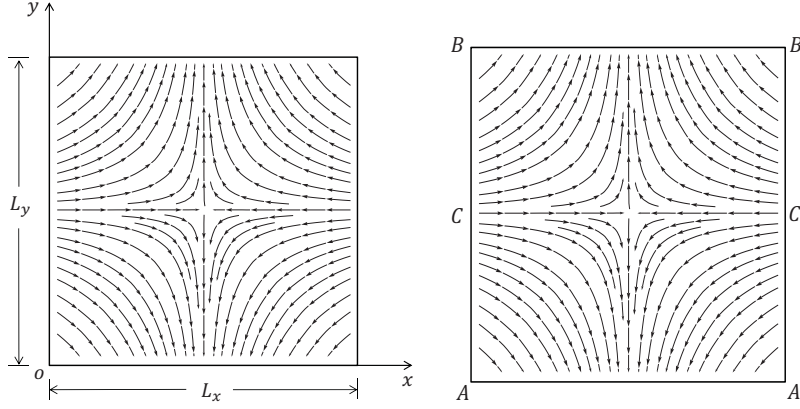


Figure 1: The initial potential flow entering through both the left AB and right $A'B'$ inlet boundaries, and exiting through the AA' and BB' boundaries. The solid lines represent the streamlines and the arrows show the direction of the flow.

2.3 Equation of state

All NS equations are coupled with the Peng-Robinson (PR) equation of state (EOS) [20]

$$p = \frac{R_u T}{v_{PR} - b_{mix}} - \frac{a_{mix}}{v_{PR}^2 + 2b_{mix}v_{PR} - b_{mix}^2} \quad (5)$$

from which T and p are obtained as an iterative solution of two nonlinear equations that satisfy both the values of ρ and e as obtained from the solution of the conservation equations. In the PR EOS, v_{PR} is the PR molar volume and the molar volume $v = v_{PR} + v_s$ where v_s is the volume shift computed to improve the accuracy of the PR EOS for high-pressure conditions [21], while the terms a_{mix} and b_{mix} are functions of T and X_i [11].

3 Initial profile: Inviscid incompressible potential flow

The initial profiles correspond to a two-dimensional potential flow in which two opposing streams, each of constant density and composition, are injected from the two boundaries AB and $A'B'$ of length L_y in the x -direction; the streams exit the domain through the two boundaries AA' and BB' of length L_x at the y -direction as illustrated in Fig. 1. Reference quantities (subscript ref) constant in time are first specified at the left (superscript l) and the right (superscript r) boundary points C and C' . The reference pressures at the two inlets are set $p_{ref}^l = p_{ref}^r = p_{ref}$, so that for the initial flow, the stagnation point (S) is always located at the centerline with $x_S = L_x/2$ and also $y_S = L_y/2$.

The initial density and mass fraction fields are given as

$$[\rho^0(x, y), Y_n^0(x, y)] = \begin{cases} [\rho_{ref}^l, Y_{n,ref}^l] & \text{if } 0 \leq x < L_x/2, \forall y \\ [\rho_{ref}^r, Y_{n,ref}^r] & \text{if } L_x/2 < x \leq L_x, \forall y \end{cases}, \quad (6)$$

where a discontinuity arises in $\rho^0(x, y)$ and $Y_n^0(x, y)$ at $x = L_x/2, \forall y$ when $\rho_{ref}^l \neq \rho_{ref}^r$ and

$Y_{n,ref}^l \neq Y_{n,ref}^r$. The components of the initial velocity field are

$$u_x^0(x, y) = -\frac{2\kappa(x - L_x/2)}{1 + \sqrt{\rho_{ref}^l/\rho_{ref}^r}}, \quad 0 \leq x < L_x/2; \quad u_x^0(x, y) = -\frac{2\kappa(x - L_x/2)}{1 + \sqrt{\rho_{ref}^r/\rho_{ref}^l}}, \quad L_x/2 < x \leq L_x \quad (7)$$

$$u_y^0(x, y) = \frac{2\kappa(y - L_y/2)}{1 + \sqrt{\rho_{ref}^l/\rho_{ref}^r}}, \quad 0 \leq x < L_x/2; \quad u_y^0(x, y) = \frac{2\kappa(y - L_y/2)}{1 + \sqrt{\rho_{ref}^r/\rho_{ref}^l}}, \quad L_x/2 < x \leq L_x \quad (8)$$

where κ is the strain rate. $u_x^0(x, y)$ is continuous $\forall(x, y)$, while $u_y^0(x, y)$ has a discontinuity at $x = L_x/2, \forall y$ when $\rho_{ref}^l \neq \rho_{ref}^r$.

Using (i) the common reference pressure, p_{ref} , of points C and C' , (ii) the Bernoulli equation which holds for inviscid incompressible flows and (iii) the fact that for irrotational (i.e. potential) flows the total pressure, as given by the Bernoulli equation, is the same for all points of the flow (otherwise the Bernoulli equation would only hold along a streamline), we obtain the initial pressure field, p^0 , as

$$p^0(x, y) = p_{ref} + \frac{1}{2}\rho_{ref}^l \left[(u_x^0(x_C, y_C))^2 + (u_y^0(x_C, y_C))^2 \right] - \frac{1}{2}\rho_{ref}^l \left[(u_x^0(x, y))^2 + (u_y^0(x, y))^2 \right], \quad (9)$$

for $0 \leq x < L_x/2, \forall y$, where $x_C = 0$ and $y_C = L_y/2$, while for $L_x/2 < x \leq L_x, \forall y$

$$p^0(x, y) = p_{ref} + \frac{1}{2}\rho_{ref}^r \left[(u_x^0(x_{C'}, y_{C'}))^2 + (u_y^0(x_{C'}, y_{C'}))^2 \right] - \frac{1}{2}\rho_{ref}^r \left[(u_x^0(x, y))^2 + (u_y^0(x, y))^2 \right], \quad (10)$$

where $x_{C'} = L_x$ and $y_{C'} = L_y/2$.

By construction, the initial potential flow satisfies the steady-state incompressible Euler's equations. The availability of $p^0(x, y), \rho^0(x, y), Y_1^0(x, y), \dots, Y_N^0(x, y)$ in conjunction with the EOS allows the determination of the initial temperature field of the flow, $T^0(x, y)$. With the calculated $T^0(x, y)$, the initial specific internal energy field is obtained. It follows that the initial field of conservative variables, $\tilde{U}^0(x, y)$, can then be readily constructed.

Finally, we note that for the counterflow configuration the use of a potential flow as initial flow is consistent with the fact that even when starting computations with a plug flow (i.e. zero y -components of the velocity vector at the inlets), the flow quickly converges to a potential type.

4 Boundary conditions

4.1 Inflow boundary conditions

Instead of explicitly imposing timewise constant boundary values (also known as hard BCs) for the conservative variables at the two inlets AB and $A'B'$, we impose the steady-state NS compressible form of the conservation equations for $\rho, \rho u_x, \rho u_y, \rho Y_1, \dots, \rho Y_{N-1}$. Using these equations as BCs means that the initial values imposed on the inlets AB and $A'B'$ for these variables are implicitly constrained to be constant with time. Most importantly, the transverse terms that give rise to multi-directional effects at the inflow boundaries are inherently present in the BCs. In addition to the above BCs, the thermodynamic computation of the energy $\rho e_t = \rho \bar{e}_t(T(x, y), p(x, y), Y_1(x, y), \dots, Y_N(x, y))$ is used for the boundary values of ρe_t at the two inlets, where \bar{e}_t is calculated using the

current values of $\rho, \rho u_x, \rho u_y, \rho Y_1, \dots, \rho Y_{N-1}$ and T is obtained from the EOS, so that the values of $\rho \bar{e}_t$ are readily available.

By construction, the initial values of $\rho, \rho u_x, \rho u_y, \rho Y_1, \dots, \rho Y_{N-1}$ at the inlets (see Section 3) satisfy the Euler instead of the NS steady-state equations. Since the inlet boundaries are usually located away from the flame, these initial values provide a good initial guess for the NS steady-state equations which can be corrected [22] to account the viscous and species mass-flux effects.

4.2 Outflow boundary conditions

At the outflow boundaries $A'A$ and BB' , the solution satisfies the unsteady compressible, reactive flow NS equations since the conditions there are the outcome of the processes taking place in the interior of the domain. At these boundaries we assume that p stays constant with time, taking the value initially provided by the Bernoulli equation.

5 Numerical scheme

An eight-order explicit finite-difference scheme is used for the spatial derivatives. After spatial discretization, the steady NS equations become algebraic equations at a node, whereas the unsteady NS equations become ordinary differential equations at a node. As a result, at the nodes of the inflow boundaries AB and $A'B'$, the BCs are numerically of algebraic type. In addition, auxiliary ghost points can be used from the left of the boundary AB and the right of the boundary $A'B'$ (since the solution is known there) to enhance the finite difference approximation of the spatial derivatives in those equations. At the nodes of outflow boundaries $A'A$ and BB' , the BCs are of differential type and one-sided finite differencing is used.

The resulting numerical system of differential-algebraic equations [23] is integrated in time with the differential-algebraic solver IDA of the SUNDIALS suite [24]. The integration method used in IDA is a variable-order, variable-coefficient BDF (Backward Differentiation Formula), in fixed-leading-coefficient form where the order of the method varies between 1 and 5. The BDF method can handle the stiffness introduced in the numerical integration of the NS equations due to the presence of chemical source terms. IDA supports parallel computations through the message passing interface (MPI) protocol and provides a routine that computes consistent initial conditions from a users' initial guess [22, 25].

6 Reproducing potential flows

To validate the proposed differential-algebraic BCs of Section 4, we consider two symmetric non-reacting potential flows where either H_2 or O_2 enters from both inlets. The goal is to numerically reproduce these two steady-state potential flows at computational times characteristic to reaction/diffusion problems.

Table 1: Inflow conditions at C and C' (see the right part of Fig. 1) for two H_2 and one O_2 simulations. N_x and N_y are the number of points in the x and y directions. $L_x = L_y = 10$ mm.

Case	Species	ρ_{ref} (kg/m ³)	T_{ref} (K)	p_{ref} (bar)	κ (s ⁻¹)	N_x	N_y
A	H ₂	0.08077	300	1	2×10^3	104	104
B	H ₂	0.08077	300	1	4×10^3	144	144
-	O ₂	1.2837	300	1	2×10^3	200	200

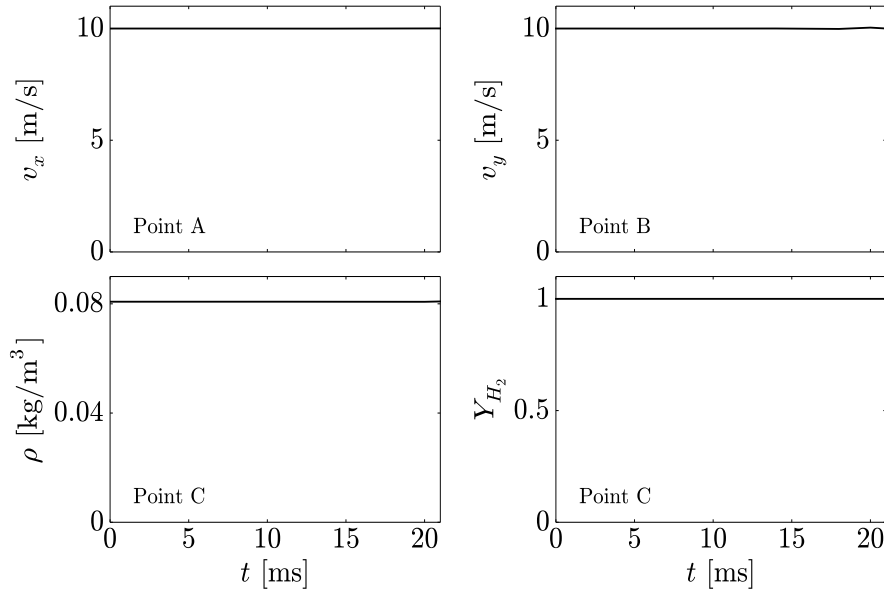


Figure 2: Temporal variation of ρ , v_x , v_y , p and Y_{H_2} at inlet boundary points for Case A of Table 1. The labeling of the points refers to the right part of Fig. 1.

6.1 The H_2 symmetric potential flow

For the symmetric H_2 potential flow, the two situations considered differ in the imposed strain rates (see Table 1). Due to space constraints, we only show below the temporal variation of the inlet boundary points for case A (Fig. 2) and the spatial variation of primitive variables at $t = 6$ ms for case B (Fig. 3). Figure 2 shows the temporal evolution of the boundary values of ρ , v_x , v_y and Y_{H_2} at points on the left inlet boundary; the prescribed initial boundary values are excellently maintained by the imposed NS steady-state BCs at the two inlets AB and $A'B'$. Figure 3 illustrates for case B the initial ($t = 0$ ms) spatial variation of ρ , v_x , v_y , p and Y_{H_2} for x -sections of the computational domain and the spatial variation of the same variables obtained at $t = 6$ ms. Clearly, the steady-state potential flow is accurately reproduced numerically in all respects for the larger κ value.

6.2 The O_2 symmetric potential flow

For the symmetric O_2 potential flow the inflow conditions and computational mesh are given on Table 1. The results of the simulation for O_2 represent a simulation performed with a fluid having a density of $\mathcal{O}(10)$ larger compared to that of H_2 used in the previous two simulations. The results are not illustrated, but they show the same high fidelity in maintaining the imposed initial potential flow as in the H_2 simulations.

7 Summary and conclusions

New BCs have been developed for the counterflow configuration that provide a very concise framework inherently accounting for the multi-directional character of the flow at the boundaries. Upon discretization of the steady-state NS equations, the BCs at the inflow boundaries are of algebraic type, whereas upon discretization of the unsteady NS equations, those at the outflow boundaries are of differential type. This formulation of the numerical BCs as differential-algebraic ones re-

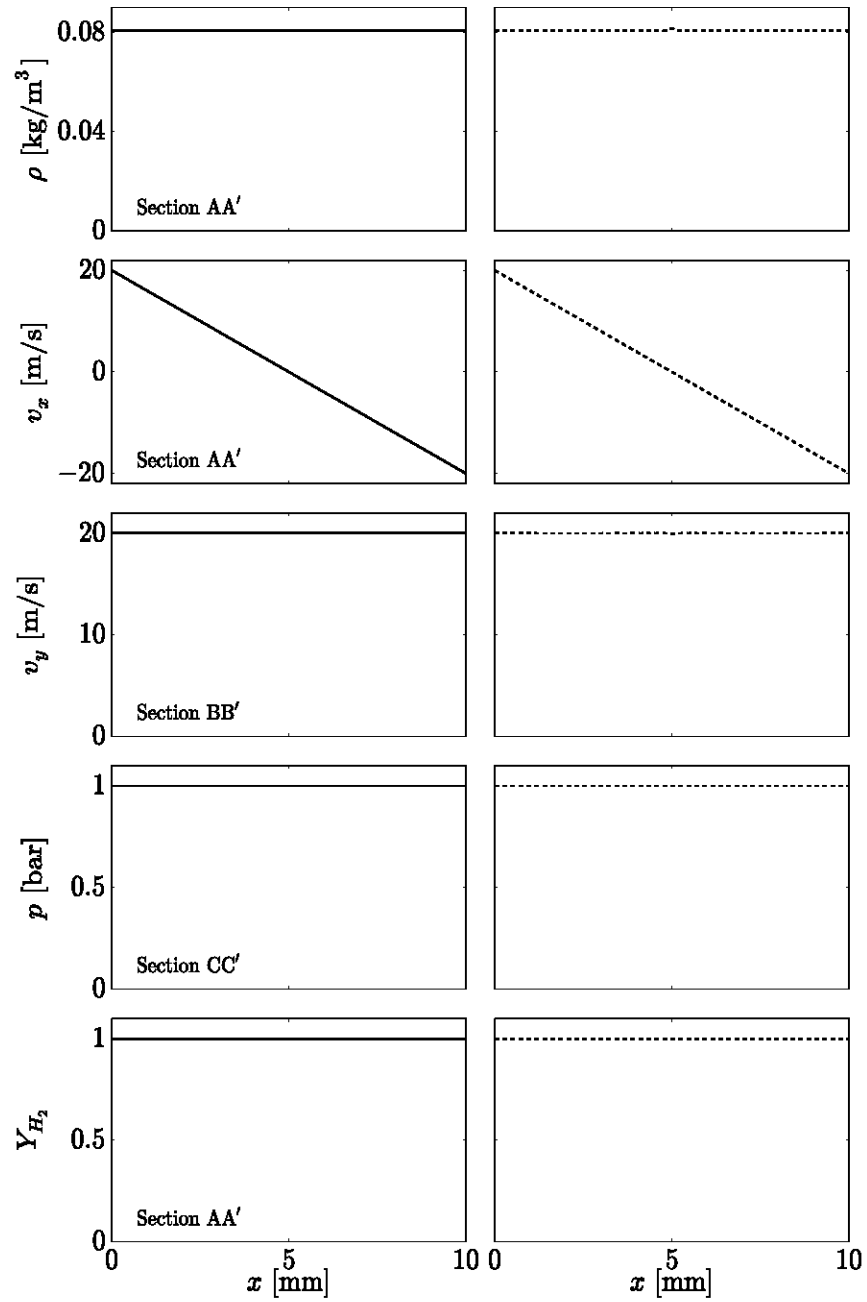


Figure 3: Spatial variation of ρ , v_x , v_y , p and Y_{H_2} for Case B of Table 1. The labeling of the sections refers to the right part of Fig. 1. Left column: $t = 0$ ms. Right column: $t = 6$ ms.

quires the use of a numerical integration software capable of handling initial-value problems for differential-algebraic systems of equations [24].

For the non-reactive-flow validation of the differential-algebraic BCs, two symmetric non-reacting potential flows were considered with either H_2 or O_2 as injected species from both inlets. For H_2 , two different strain rates cases were examined whereas for O_2 only one strain rate flow is simulated. Irrespective of the species or the strain rate, the initial potential flow was reproduced with high fidelity over the entire computational domain without numerical artifacts, i.e. without use of dissipative filters or introduction of relaxation constants into the BCs.

Acknowledgements

This work was performed at the California Institute of Technology and the Jet Propulsion Laboratory Division of the California Institute of Technology, and was sponsored by United States Army Research Office, with Dr. Ralph Anthenien as contract monitor. Supercomputing time from the DoD HPCMP Open Research Systems and JPL/NASA is gratefully acknowledged.

References

- [1] H. Tsuji, Prog. Energ. Combust.8(2) (1982) 93-119.
- [2] E. Mastorakos, A. Taylor, J. Whitelaw, Combust. Flame 91(1) (1992) 55-64.
- [3] R. Seiser, H. Pitsch, K. Seshadri, W. Pitz, H. Gurrán, Proc. Combust. Inst. 28(2) (2000) 2029-2037.
- [4] G. Ribert, N. Zong, V. Yang, L. Pons, N. Darabiha, S. Candel, Combust. Flame 154(3) (2008) 319-330.
- [5] M.S. Agathou, D.C. Kyritsis, Fuel 90(1) (2011) 255-262.
- [6] G. Lacaze, J.C. Oefelein, Combust. Flame 159(6) (2012) 2087-2103.
- [7] C.S. Yoo, Y. Wang, A. Trouvé, H.G. Im, Combust. Theory Model. 9(4) (2005) 617-646.
- [8] B.G. Sarnacki, G. Esposito, R.H. Krauss, H.K. Chelliah, Combust. Flame 159 (2012) 1026-1043.
- [9] R.F. Johnson, A.C. VanDine, G.L. Esposito, H.K. Chelliah, Comb. Sci. Techn. 187 (2015) 1-23.
- [10] T.J. Poinso, S.K. Lele, J. Comput. Phys.101(1) (1992) 104-129.
- [11] E. Masi, J. Bellan, K. Harstad, N..Okong'o, J. Fluid Mech. 721 (2013) 578-626.
- [12] J. Keizer, Statistical Thermodynamics of Nonequilibrium Processes, Springer-Verlag, New York, 1987.
- [13] K. Harstad, J. Bellan, Int. J. Heat Mass Tran. 41(22) (1998) 3537-3550.
- [14] K. Harstad, J. Bellan, Int. J. Multiph. Flow 26(10) (2000) 1675-1706.
- [15] K. Harstad, J. Bellan, J. Chem. Phys. 120(12) (2004) 5664-5673.
- [16] H. Grad, Commun. Pur. Appl. Math. 2(4) (1949) 331-407.
- [17] R.C. Reid, J.M. Prausnitz, B.E. Poling, The properties of gases and liquids, McGraw Hill, 4th edition, 1987.
- [18] K. Harstad, J. Bellan, Ind. Eng. Chem. Res. 43(2) (2004) 645-654.
- [19] J. Hirshfelder, C. Curtis, R. Bird, Molecular Theory of Gases and Liquids, John Wiley and Sons, 1964.
- [20] D.-Y. Peng, D. Robinson, Ind. Eng. Chem. Res. 15(1) (1976) 59-64.
- [21] K. Harstad, R.S. Miller, J. Bellan, AIChE J. 43(6) (1997) 1605-1610.
- [22] P.N. Brown, A.C. Hindmarsh, L.R. Petzold, SIAM J. Sci. Comput. 19(5) (1998) 1495-1512.
- [23] K.E. Brenan, S.L. Campbell, L.R. Petzold, Numerical Solution of Initial-Value Problems in Differential-Algebraic Equations, SIAM, 1996.
- [24] A.C. Hindmarsh, P.N. Brown, K.E. Grant, S.L. Lee, R. Serban, D.E. Shumaker, C.S. Woodward, C. S., ACM Trans. Math. Softw. 31(3) (2005) 363-396.

Sub Topic: Laminar Flames

- [25] A.C. Hindmarsh, R. Serban, A. Collier, A., User Documentation for IDA v2.7.0, Tech. Rep. UCRL-SM-208112, Lawrence Livermore National Laboratory, Livermore, CA, 2012.